PNAS RESEARCH ARTICLE | MEDICAL SCIENCES OPEN ACCESS

COVID-19-related hyperglycemia is associated with infection of hepatocytes and stimulation of gluconeogenesis

Ester A. Barreto[a,b], Amanda S. Cruz[a,b], Flavio P. Veras[a,b], Ronaldo Martins[c], Rafaella S. Bernardelli[d], Isadora M. Paiva[a,b], Thais M. Lima[e], Youvika Singh[f], Raphael C. Guimarães[g], Samara Damasceno[a,b], Nayara Pereira[a,b], João Manoel Alves[a,b], Tiago T. Gonçalves[a,b], Julia Forato[h], Stéfanie P. Muraro[h], Gabriela F. Souza[h], Sabrina Setembre Batah[e], José L. Proenca-Modena[h,i], Marcelo A. Mori[g,i,j], Fernando Q. Cunha[a,b], Paulo Louzada-Junior[b,k], Thiago M. Cunha[a,b], Helder I. Nakaya[b,f], Alexandre Fabro[e], Renê D. R. de Oliveira[k], Eurico Arruda[c], Rosângela Réa[d,l], Álvaro Réa Neto[d,l], Miguel M. Fernandes da Silva[l], and Luiz Osório Leiria[a,b,1]

Edited by David E. Cohen, Brigham and Women's Hospital, Boston, MA; received October 7, 2022; accepted April 19, 2023 by Editorial Board Member C. Ronald Kahn

Occurrence of hyperglycemia upon infection is associated with worse clinical outcome in COVID-19 patients. However, it is still unknown whether SARS-CoV-2 directly triggers hyperglycemia. Herein, we interrogated whether and how SARS-CoV-2 causes hyperglycemia by infecting hepatocytes and increasing glucose production. We performed a retrospective cohort study including patients that were admitted at a hospital with suspicion of COVID-19. Clinical and laboratory data were collected from the chart records and daily blood glucose values were analyzed to test the hypothesis on whether COVID-19 was independently associated with hyperglycemia. Blood glucose was collected from a subgroup of nondiabetic patients to assess pancreatic hormones. *Postmortem* liver biopsies were collected to assess the presence of SARS-CoV-2 and its transporters in hepatocytes. In human hepatocytes, we studied the mechanistic bases of SARS-CoV-2 entrance and its gluconeogenic effect. SARS-CoV-2 infection was independently associated with hyperglycemia, regardless of diabetic history and beta cell function. We detected replicating viruses in human hepatocytes from *postmortem* liver biopsies and in primary hepatocytes. We found that SARS-CoV-2 variants infected human hepatocytes in vitro with different susceptibility. SARS-CoV-2 infection in hepatocytes yields the release of new infectious viral particles, though not causing cell damage. We showed that infected hepatocytes increase glucose production and this is associated with induction of PEPCK activity. Furthermore, our results demonstrate that SARS-CoV-2 entry in hepatocytes occurs partially through ACE2- and GRP78-dependent mechanisms. SARS-CoV-2 infects and replicates in hepatocytes and exerts a PEPCK-dependent gluconeogenic effect in these cells that potentially is a key cause of hyperglycemia in infected patients.

SARS-CoV-2 | liver | glucose

Significance

Hyperglycemia is a prevalent complication in hospitalized COVID-19 patients that occurs regardless of the diabetes history and is associated with a worse clinical outcome. In this study, we found that COVID-19 is independently associated with in-hospital hyperglycemia and that SARS-CoV-2 is capable of infecting hepatocytes and stimulate these cells to produce glucose through gluconeogenesis. Moreover, our data suggest that SARS-CoV-2's entrance in hepatocytes is partially mediated by the cooperation between GRP78 and ACE2 cotransporters. Our data provide mechanistic insights on how COVID-19 pathophysiology impact glucose metabolism and shed light on the importance of in-hospital control of hepatic glucose production as a means to achieve better clinical outcome in COVID-19 patients.

Diabetes constitutes a major risk factor for the development of severe forms of COVID-19 (1, 2). Moreover, several studies indicate that the incidence of hyperglycemia in COVID-19 patients is associated with longer periods of hospitalization and with worse clinical outcome (3, 4). Intriguingly, hyperglycemia resulting from COVID-19 is also prevalent in patients without a history of diabetes (5), which suggests that like other RNA viruses, SARS-CoV-2 may directly interfere with glucoregulatory pathways, resulting in increased blood glucose levels.

Other groups have tried to address the mechanistic link between the viral infection and hyperglycemia (6, 7). Beta cell infection and damage induced by SARS-CoV-2 was shown in vitro, but its clinical relevance is still controversial. On the contrary, COVID-19 is also associated with the onset of insulin resistance (8), which potentially contributes to the imbalance in blood glucose control. Since other viral infections caused by RNA viruses such as hepatitis C and B (HCV and HBV, respectively) can induce hepatic glucose production through the stimulation of gluconeogenesis in hepatocytes (9, 10), it is plausible that SARS-CoV-2 could act similarly.

A few studies have demonstrated by immunofluorescence in *postmortem* biopsies that SARS-CoV-2 can indeed infect hepatocytes and cause liver damage (11, 12). In addition, GP73 is a gluconeogenic protein secreted under SARS-CoV-2 infection and capable of stimulating gluconeogenesis in Huh7 hepatoma cell line (13). However, it is still unknown whether SARS-CoV-2 can directly stimulate glucose production in hepatocytes. Moreover, the mechanism of infection of hepatocytes and whether such an infection is productive or not are important questions that remain to be addressed.

The authors declare no competing interest.

This article is a PNAS Direct Submission. D.E.C. is a guest editor invited by the Editorial Board.

[1]To whom correspondence may be addressed. Email: luizleiria@usp.br.

This article contains supporting information online at https://www.pnas.org/lookup/suppl/doi:10.1073/pnas.2217119120/-/DCSupplemental.

Published May 15, 2023.

In the present study, we combined a retrospective clinical study with ex vivo and in vitro experimental strategies to show that SARS-CoV-2 infects hepatocytes through ACE2 and GRP78 mediated cotransport, thus yielding an increase in hepatic glucose production in a PEPCK-dependent manner.

Methods

Human Subjects of Clinical Study. Clinical data were collected from 269 patients from the Clinics Hospital of Ribeirão Preto Medical School of the University of Sao Paulo (HCFMRP-USP) admitted to ICUs and regular bed and 663 patients from Center for Study and Research in Intensive Care Medicine (CEPETI) of Curitiba. The inclusion criteria were patients with suspected COVID-19 hospitalized from March to August 2020 who underwent a SARS-CoV-2 PCR test and had the measurement of blood glucose levels at admission. Given the dates of hospitalization, we assume that our clinical data only include patients infected with the original variant. We excluded patients with liver dysfunction, HIV infection, and cancer (*SI Appendix*, Fig. S1). COVID-19-positive patients were those with a positive SARS-CoV-2 PCR test, while those with suspected COVID-19 based on clinical presentation, but subsequently had a negative SARS-CoV-2 PCR test, were defined as COVID-19 negative. The data were recorded in REDCap software, which included medical history, laboratory information, and daily maximum glycemia value until discharge or death. Diabetes was assessed according to previous history or antidiabetic drug use. Severity of the disease at presentation was estimated by the Sequential Organ Failure Assessment (SOFA) score at admission, which assesses organ dysfunction. A higher SOFA score is associated with higher probability of mortality. The protocol approval numbers of the Human Research Ethics Committee of HCFMRP-USP and CEPETI were 4,763,062 and 3,573,668, respectively. Eligible patients were invited to participate in the study. Informed consent was waived for this study due to its retrospective nature.

Serum Analysis. We used serum samples from a subgroup of nondiabetic patients from the HCFMRP-USP site, collected at their admission in the hospital, in order to measure glucometabolic profile, thus assessing whether the glucose increase in COVID-19 patients was due to beta cell dysfunction. The quantifications were performed using the following ELISA kits: c-peptide (80,954), glucagon (81,520), and glycated serum protein (80,109) (ChrystalChem™).

Immunofluorescence and Confocal Microscopy. Slides of liver tissue section from four nondiabetic COVID-19 fatal cases from HCFMRP-USP were fixed with 4% PFA, blocked with blocking buffer (Millipore, 20773-M), and stained with the primary antibodies (PA). The slides were washed with Tris-Buffered Saline with Tween-20 (TBS-T) and incubated with secondary antibodies (SA). Autofluorescence was quenched using Quenching Kit (Vector Laboratories™, SP-8400-15). Cells were fixed using 3.7% formaldehyde and blocked with 0.1% tween-20 plus 1% BSA in PBS. The cells were incubated with PA, washed with PBS, and incubated with SA. The slides were then mounted using the medium with DAPI (Vector Laboratories™, H-1200-10). Images were acquired by Axio Observer combined with LSM 780 confocal microscope (Carl Zeiss™) and analyzed with Image J. Antibodies were indicated in *SI Appendix*, Table S2.

Cell Culture and Treatments. Human primary hepatocytes (Lonza™, HUCPG) from three different donors (HUM193101, HUM17299A, and HUM183001) were thawed and plated using appropriated media (Lonza™, MCHT50 and MP100) in collagen-coated plates (Corning™, 354,236). HUCPG cells were cultured in appropriate medium (Lonza™, CC-3198) and Vero E6 and Vero CCL-81 cells in DMEM high-glucose medium (CultiLab™, 620) supplemented with 10% fetal bovine serum, FBS (Gibco™, 10,437), and 1% streptomycin/penicillin (Gibco™, 15,140). Neutralizing antibodies such as anti-ACE2 (R&D Systems™, AF933, 20 μg/mL) or the selective GRP78 antagonist HM03 (MedChemExpress™, HY-125974/5) were used for investigating viral entry mechanism.

SARS-CoV-2 Stock Propagation and In Vitro Infection. The SARS-CoV-2 Brazil/SPBR-02/2020, gamma (P1) strain MAN87209, delta, and omicron variants were used under strict BSL3 conditions (14). Viral inoculum (1:100 ratio) was added in Vero CCL-81 cells and incubated (48 h) in the media without FBS under standard conditions. After confirmation of viral cytopathic effects using Olympus ix51 microscope, monolayers were harvested with a cell scraper, snap-frozen in liquid nitrogen, thawed, and clarified by centrifugation (1,000 × g). Supernatants were aliquoted and stored at −80 °C until use. Virus titration was performed on Vero CCL81 cells using standard limiting dilution to determine the 50% tissue culture infectious dose ($TCID_{50}$) of viral stock. Cells were incubated with SARS-CoV-2 strains according to the desired viral MOI in culture medium without BSA for 1h at RT on agitation in orbital shaker in a BSL3 laboratory. Then, the cells were washed with PBS and incubated with culture medium under standard conditions for time indicated in text.

Quantification of SARS-CoV-2 Viral Load and Gene Expression by RT-qPCR. RNA was extracted by the Trizol® (Invitrogen™) and converted to cDNA according to manufacturer's instructions (Applied Biosystems™, 4,374,966). SARS-CoV-2 viral load was performed by quantification of the N1 gene using the QuantStudio five Real-Time PCR System (Applied Biosystems™). To access the N1 number of copies, a standard curve was made using a plasmid (PTZ57R/T CloneJet™ Cloning Kit, ThermoFisher™) in accordance with the US Centers for Disease Control (CDC). The qPCR reaction was performed. The amplification protocol was 95 °C for 10 min, followed by 40 cycles of 95 °C for 15 s, and 60 °C for 1 min. Gene expression was performed using specific primers (*SI Appendix*, Table S3) and SYBR Green/ROX (ThermoFisher™, K0223). The amplification protocol was 95 °C for 10 min, followed by 40 cycles of 95 °C for 15 s, 60° for 30 s, and 72° for 30 s. Amplification plots, melting curves, and Ct values were obtained using the CFX Manager (Bio-Rad). Relative gene expression was calculated using $2\text{-}\Delta\Delta Ct$.

Plaque-Forming Unit (PFU) Assay. Vero E6 cells were incubated with serial dilutions of supernatant of infected HUCPG for 1 h under RT. Then, overlay medium containing DMEM, 2.5% carboxymethylcellulose, and 2% FBS was added followed by 4-d incubation under standard conditions. Then, cells were fixed (10% formalin/PBS) and stained with 0.5% w/v crystal violet solution, and then washed to reveal the plates.

Hepatocyte Viability. Cell viability was measured using Cytotox assay (Promega™, G1782), while quantification of ALT (Labtest™, 108) and AST (Labtest™, 109) was performed according to kit instructions.

Gluconeogenesis Assay. Infected HUPCG cells were incubated for 1 h with gluconeogenesis medium (8.3 g/L DMEM Sigma, D5030; 20 mM lactate; 2 mM pyruvate; 4 mM L-glutamine; 3.7 g/L of sodium bicarbonate) and glucagon (50 nM) was added in positive control. Then, supernatant was used to evaluate glucose levels according to kit instructions (EnzyChrom™ Glucose Assay Kit, EBGL-100). For PEPCK activity assay, infected cells were washed with PBS and proceeded according to the manufacturer instructions (LSBio™, LS-K444-100).

Single-Cell RNA-Seq Analysis. Liver scRNAseq data were downloaded from GEO (GSE115469) (15). We analyzed 8,135 liver cells from five patients using Seurat-R package v4.0.0 (PMID: 34062119). To maximize the quality, we discarded cells with less than 200 genes and greater than 4,000 genes and cells that express > 5% mitochondrial genes. Highly variable genes were identified using the "vst" method from the Seurat package. Gene expression matrices were scaled and centered, and principal component analysis was performed. Cells were clustered using the Louvain algorithm and visualized by tSNE using top 10 PCs. Clusters were annotated manually using specific markers (*SI Appendix*, Table S4).

Western Blotting. Cells were lysed in RIPA buffer (Cell Signaling™, 9,806) with protease inhibitor (Roche™, 11836170001). After centrifugation at 14,000 × g for 20 min at 4 °C, proteins were fractionated through SDS-PAGE (sodium dodecyl sulfate–polyacrylamide gel electrophoresis) on 8% acrylamide gel and transferred to nitrocellulose membranes (Bio-Rad™), followed by blocking in TBST-T with 5% low-fat milk, and then incubated with the PA overnight at 4 °C followed by 1 h of SA incubation. Antibodies are indicated in *SI Appendix*, Table S2.

Statistical Analysis. Statistical analysis was determined by one-way ANOVA followed by Tukey's post-hoc test. Unpaired *t* test was used for continuous data if they meet the criteria for Gaussian distribution or the Mann–Whitney test if otherwise. To assess the association between positive COVID-19 and the incidence of severe hyperglycemia (glucose blood levels of 300 mg/dL or above), we calculated Kaplan–Meyer estimates and compared the probability of the outcome using the log-rank test. Then, we performed a Cox proportional hazard regression analysis adjusted for age, sex, body mass index (BMI), diabetes, and use of corticosteroid (model 1). We further adjusted for the SOFA score at admission

(model 2) to account for severity of the disease as a potential confounder. We considered statistically significant $P < 0.05$. Analyses and graphs were performed using Stata version 15.1 (Stata Corp, College Station™, TX) or GraphPad Prism™ 8.4.2 software.

Results

Baseline Data from the Retrospective Cohort Study. In our cohort study, we found that a comparable proportion of COVID-19-positive and -negative patients (85.8% and 80.3%, respectively) included in this study were admitted to the intensive care unit (ICU), while others were kept at wards (Table 1). Both groups were similar in gender, age, and SOFA index. Glycemia at admission was significantly higher in the COVID-19-positive group ($P = 0.003$). Interestingly, we found a slightly higher incidence of obesity ($P < 0.001$) along with elevated average body weight ($P < 0.001$) and BMI ($P = 0.001$) in the COVID-19-positive versus the COVID-19 negative group (Table 1), while no difference in diabetes prevalence was observed. Also, fewer smokers ($P < 0.001$) and more cases of chronic kidney disease ($P = 0.021$) were found in the COVID-19-positive group (Table 1). Laboratory findings at admission revealed no differences in ALT, AST, and creatinine levels between groups, although the C-reactive protein was elevated in positive cases (Table 1). As expected, partial pressure of oxygen (PaO_2) was found to be lower in the COVID-19-positive group ($P < 0.001$).

COVID-19 Is an Independent Risk Factor for the Development of Hyperglycemia. We assessed whether patients with COVID-19 were more prone to develop hyperglycemia during hospitalization. Daily maximum glycemia was recorded in all patients during hospital stay. We considered severe hyperglycemia as any value above 300 mg/dL, which was associated with substantial increase in hospital mortality in critically ill patients (16). The COVID-19-positive patients exhibited higher incidence of hyperglycemic episodes over their hospital stay (Fig. 1*A*), which occurred regardless of their diabetes status (Fig. 1 *B* and *C*). To test whether COVID-19 is an independent causative factor for hyperglycemia, a Cox regression was performed. The hazard ratio (HR) for developing hyperglycemia among COVID-19-positive versus COVID-19-negative was 2.27 (95% CI, 1.52 to 3.39). After adjustment for sex, age, gender, BMI, diabetes, and corticosteroid use, we found an HR of 2.89 (95% CI, 1.69 to 4.92), while the additional adjustment for SOFA score rendered an HR of 2.62 (95% CI, 1.45 to 4.72) (Table 2). This association remained similar in the corticosteroid-naïve patients with an adjusted HR: 2.45 (95%CI 1.20, 4.98). When analyzed separately, the two cohorts displayed similar results as shown for the merged population (Table 2). Of note, BMI was not independently associated with the incidence of hyperglycemia and there was no significant interaction between COVID-19 and BMI (*SI Appendix*, Table S1). These data indicate that COVID-19 holds a strong and independent correlation with the occurrence of hyperglycemia.

Glucometabolic Changes in Nondiabetic COVID-19 Patients Did Not Involve Pancreatic Failure. Next, we interrogated whether hyperglycemia was due to endocrine pancreas damage. Serum collected on admission from a subgroup of 119 nondiabetic patients from HCFMRP-USP site were categorized as COVID-19 negative (n = 17), normoglycemic COVID-19 positive (n = 39), and COVID-19 positive with high blood glucose (n = 63), with 130 mg/dL as the cutoff value to distinguish normal from high blood glucose (Fig. 1*D*). These patients were evaluated for glucagon, C-peptide, and glycated protein serum levels. Serum was collected on the day of hospital admission. COVID-19-positive patients with high blood glucose levels displayed increased C-peptide, glucagon, and glycated protein levels in comparison to COVID-19-negative patients (Fig. 1 *E*–*G*). They also had higher levels of C-peptide and glycated serum proteins, but not glucagon, when compared to normoglycemic COVID-19-positive patients, indicating that these patients normally secrete insulin in response to hyperglycemia, at least by the time of the admission.

Detection of SARS-CoV-2 Viral Particles in the Liver. Next, we interrogated whether SARS-CoV-2 could cause hyperglycemia by stimulating hepatic glucose production. First, we investigated the presence of SARS-CoV-2 in *postmortem* liver samples from four

Table 1. Clinical and etiological characteristics of patients hospitalized with suspected COVID-19

	Negative COVID-19 n = 203	Positive COVID-19 n = 647	*P* value
Age, y	62.16 ± 19.57	59.94 ± 15.55	0.10
Women, n(%)	106 (52.2%)	289 (44.7%)	0.06
Weight, Kg	76.15 ± 23.30	83.76 ± 20.55	<0.001
BMI, Kg/m2	27.95 ± 8.04	30.23 ± 6.77	0.001
Obesity, n(%)	34 (26.6%)	224 (47.8%)	<0.001
Diabetes, n(%)	52 (25.7%)	199 (30.9%)	0.16
Smoking, n(%)			<0.001
No	131 (65.8%)	492 (79.5%)	
Current smoker	35 (17.6%)	35 (5.7%)	
Former smoker	33 (16.6%)	92 (14.9%)	
Chronic kidney disease, n(%)			0.021
No	188 (93.1%)	618 (95.8%)	
Without dialysis	13 (6.4%)	17 (2.6%)	
With dialysis	1 (0.5%)	10 (1.6%)	
SOFA	6.34 ± 3.47	6.38 ± 3.49	0.91
ICU admission	163 (80.3%)	555 (85.8%)	0.07
Laboratory at admission			
ALT	47.88 ± 94.21	48.84 ± 46.48	0.87
AST	53.34 ± 91.72	61.57 ± 81.25	0.32
AST/ALT ratio	1.50 ± 1.10	1.43 ± 0.79	0.44
Glycemia, mmol/L	8.96 ± 4.51	10.32 ± 5.45	0.003
Creatinine, mg/dL	1.24 ± 1.01	1.18 ± 1.17	0.59
C-reactive protein	58.53 ± 80.60	95.44 ± 87.98	<0.001
pH	7.38 ± 0.10	7.40 ± 0.10	0.016
PaO2	97.09 ± 44.67	82.39 ± 32.48	<0.001
Corticosteroid, n(%)	66 (33.0%)	324 (50.8%)	<0.001
Ribeirao city	55 (27.1%)	200 (30.9%)	0.30
Days from symptom onset	3.0 [1.0, 7.0]	7.0 [4.0, 9.0]	<0.001

Comparison was made with unpaired *t* test or Mann–Whitney test. BMI–Body mass index. SOFA–Sequential Organ Failure Assessment. ALT–Alanine transaminase. AST–Aspartate transaminase. PaO_2 –Partial pressure of oxygen.

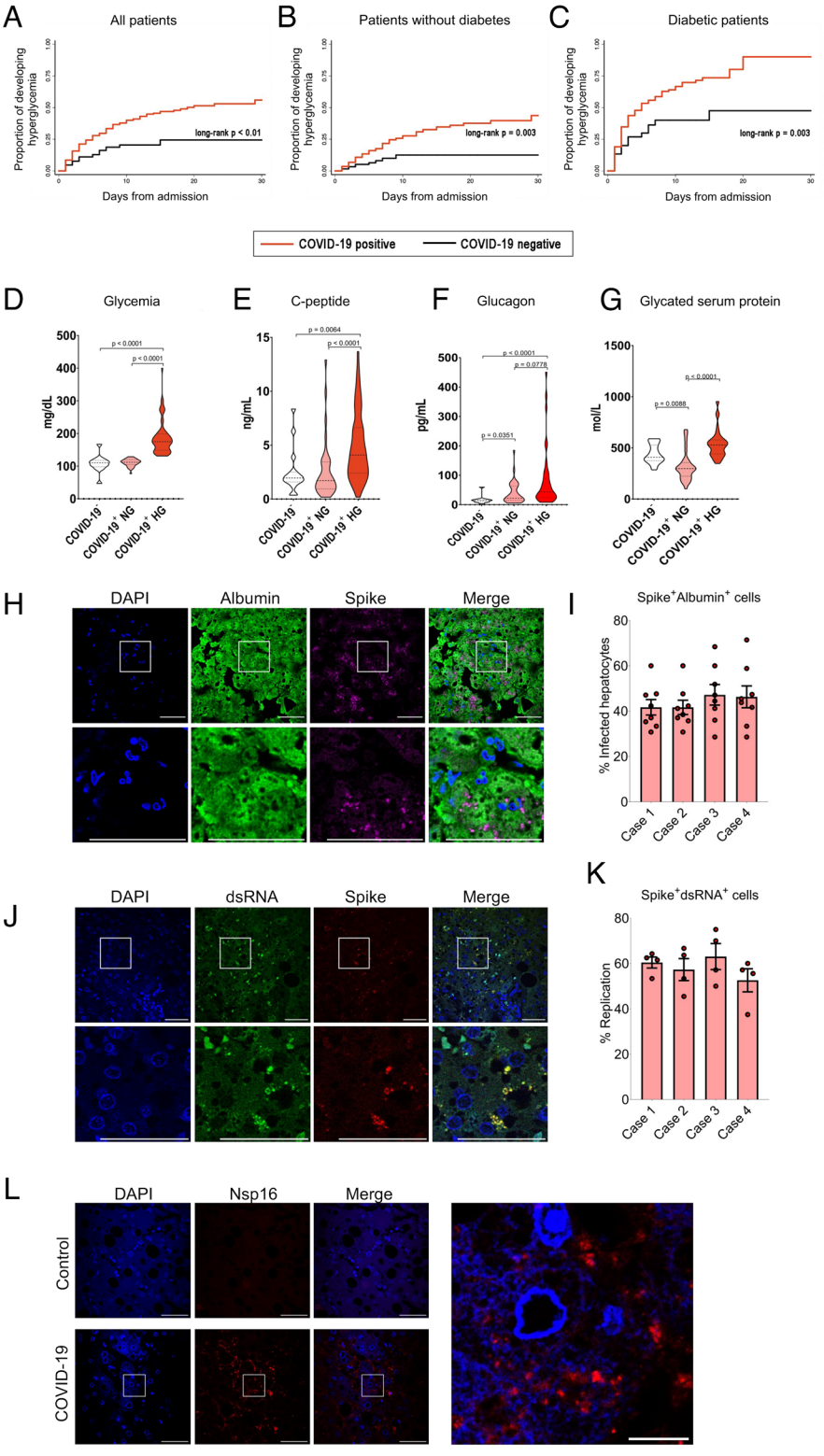

Fig. 1. Risk of hyperglycemia and glycometabolic alterations in COVID-19 cases. Kaplan–Meyer curve for the cumulative probability of COVID-19 patients developing hyperglycemia above or equal to 300 mg/dL in all patients (*A*) or categorized by the absence (*B*) and presence of diabetes (*C*). Evaluation of glycemia at admission (*D*), serum levels of C-peptide (*E*), glucagon (*F*) and glycated proteins (*G*) in serum collected at admission. ANOVA followed by Bonferroni post-hoc test was performed. (*H*) Evaluation of spike in hepatocytes. Green—albumin (hepatocytes). (Scale bar: 60 μm and 30 μm.) (crop images). (*I*) Percentage of albumin cells colocalized with spike protein in the liver of four individuals. (*J*) Evaluation of spike and double-stranded RNA in the human liver. Blue—DAPI (nuclear marker). Magenta—SARS-COV-2 spike protein. Green—J2 (dsRNA marker). (*K*) Percentage of cells with J2 and spike protein with colocalized liver tissue in four individuals' cases. (*L*) Immune staining of liver biopsies with the nonstructural viral protein NSP-16 (red). *$P < 0.05$.

nondiabetic patients of our cohort who developed hyperglycemia while at the ICU and died due to complications of COVID-19. We identified the presence of the spike protein within approximately 40% of the hepatocytes screened, which were comarked with albumin immunolabeling (Fig. 1 *H* and *I* and *SI Appendix*, Fig. S2*A*). We also found that spike protein colocalized with double-strand RNA (dsRNA), suggesting that the virus can replicate in the liver (Fig. 1 *J* and *K* and *SI Appendix*, Fig. S2*B*). Evidence of SARS-CoV-2 replication in the liver was also assessed by fluorescent in situ labeling with an antibody specific for the nonstructural protein NSP-16 (Fig. 1*L* and *SI Appendix*, Fig. S3). We observed that liver biopsies from COVID-19 patients were positive for NSP-16, which in turn were focally distributed into parenchymal hepatocytes.

SARS-CoV-2 Infect, Replicate, and Stimulate Gluconeogenesis in Primary Human Hepatocytes. Then, we sought to test whether and how SARS-CoV-2 infects primary human hepatocytes. For

Table 2. Determination of hazard ratio (HR) after Cox regression, for assessing whether there is an independent association between COVID-19 and the occurrence of in-hospital hyperglycemia

	n	HR (95% CI)	P value
All sites			
Unadjusted	752	2.27 (1.52, 3.39)	<0.001
Adjusted for model 1(*)	525	2.89 (1.69, 4.92)	<0.001
Adjusted for model 2(**)	343	2.62 (1.45, 4.72)	0.001
Ribeirão Preto site			
Unadjusted	255	3.01 (1.40, 6.52)	0.005
Adjusted for model 1(*)	170	4.03 (1.61, 10.08)	0.003
Adjusted for model 2(**)	66	2.97 (1.04, 8.54)	0.043
Curitiba site			
Unadjusted	507	1.98 (1.24, 3.18)	0.004
Adjusted for model 1(*)	355	2.10 (1.08, 4.12)	0.030
Adjusted for model 2(**)	277	2.50 (1.20, 5.18)	0.014

*Model 1: Adjusted by age, sex, BMI, diabetes, use of corticosteroid.
**Model 2: Adjusted as Model 1 + SOFA score at admission.

this purpose, we exposed the hepatocytes (Lonza, HUCPG) to the ancestral SARS-CoV-2 B lineage, here called SPBR-02, at a multiplicity of infection (MOI) of 0.1 and 1. We found that human hepatocytes are susceptible to the SARS-CoV-2 infection by detecting the presence of the spike protein within the hepatocytes using immunofluorescence or quantification of viral RNA copies (Fig. 2 *A* and *B*). Importantly, SPBR-02 was found to replicate in hepatocytes and generate infective viral particles as detected by PFU assay (Fig. 2*C*), thus corroborating our findings in liver biopsies. Surprisingly, infection with SPBR-02 did not result in cell damage as indicated by the quantification of lactate dehydrogenase (LDH), alanine aminotransferase (ALT), and aspartate aminotransferase (AST) in the medium after either 24 or 48 h post infection (Fig. 2 *D–F*). Next, we investigated whether the infection with SPBR-02 could stimulate hepatic glucose production. The virus increased glucose production in human primary hepatocytes by about twofold at 48 h post infection, in a magnitude comparable to the positive control glucagon (Fig. 2*G*), while it did not increase glucose production at 24 h post infection (*SI Appendix*, Fig. S4*A*). Interestingly, while mRNA expression of genes related to either gluconeogenesis or glycogenolysis was unchanged or even reduced upon infection with SPBR-02 (Fig. 2*H* and *SI Appendix*, Fig. S4 *B–D*), a twofold and fourfold increase in the activity of phosphoenolpyruvate carboxykinase (PEPCK), a rate-limiting enzyme for hepatic glucose production through gluconeogenesis, was observed in 0.1 and 1 MOIs, respectively, at 48 h post infection (Fig. 2*I*). In addition, we also found that the inactive SPBR-02 virus was uncapable of increasing glucose production in primary human hepatocytes (*SI Appendix*, Fig. S4*E*). Collectively, these data indicate that SARS-CoV-2 exerts a progluconeogenic effect associated with the activation of PEPCK. When infecting hepatocytes with the other three major variants of concern (gamma, delta, and omicron) at an MOI of 0.1, we found that our cells displayed comparable susceptibility to all of them (Fig. 2*J*). We also analyzed infective particle production in the supernatant from cells infected with those variants and we found that gamma and delta variants also induced plaque formation, while omicron did not (Fig. 2*K*). Similarly, to SPBR-02, infection with any of the other variants of concern did not result in cell damage as measured by LDH, ALT, and AST (*SI Appendix*, Fig. S4 *F–H*). Finally, all the variants were equally able to stimulate both hepatic glucose production and PEPCK activity (Fig. 2 *L* and *M*).

Virus Entry in Hepatocytes Partially Relies on a Short-Molecular-Weight ACE2 and the Chaperone GRP78. The role of ACE2 as a viral transporter in hepatocytes is still controversial as its RNA expression is low in such cells (17). We decided to start evaluating whether SARS-CoV-2's entry into hepatocytes might be mediated by ACE2 or other proteins by analyzing a public scRNAseq dataset obtained from a healthy human liver (15). Confirming previous findings, we also found a low expression of *ACE2* in hepatocytes, while the chaperone glucose-regulated protein 78 (GRP78, gene name *HSPA5*), was the most highly expressed transporter found in hepatocytes (Fig. 3 *A–C* and *SI Appendix*, Fig. S5 *A–E*). We further investigated the expression of ACE2 by immunofluorescence in livers from patients who died because of COVID-19. ACE2 colocalized with spike protein in hepatocytes (Fig. 3*D*). Furthermore, ACE2 detection by western blotting of primary human hepatocytes revealed that these cells express a low-molecular-weight ACE2 isoform (50 kDa) instead of the regular one (120 to 130 kDa) (Fig. 3*E*). We also decided to investigate the expression profile of GRP78, since it was the most expressed entry factor in hepatocytes. GRP78 is a chaperone that normally resides in the endoplasmic reticulum (18) but can translocate to the plasma membrane under stress (19). Moreover, GRP78 can serve as an entry factor for several viruses (20, 21). Indeed, we found that GRP78 is highly expressed in liver tissue in colocalization with spike (Fig. 3*F*).

Finally, we tested whether ACE2 and GRP78 mediate SARS-CoV-2 entry into hepatocytes. We first performed an in vitro infection on hepatocytes in which SARS-CoV-2 was in contact with the cells for only 50 min to allow for the detection of viral particles at the cell membrane, rather than inside the cell, and thus confirm whether ACE2 or GRP78 was present in cell membrane while colocalizing with spike protein. The cells were incubated with a cell membrane marker (CellMask, Invitrogen), and immunofluorescence without permeabilization was performed. We observed that both GRP78 and ACE2 were present on the cell membrane and colocalized with spike protein (Fig. 4 *A* and *B*), suggesting that both GRP78 and ACE2 are present on in hepatocyte membranes and interact with viral particles during SARS-CoV-2 adsorption.

Next, we pretreated primary hepatocytes with either neutralizing anti-ACE-2 antibody (22) or GRP78 inhibitor, HM03 (23), at different concentrations 1 h before infection. Since GRP78 is a chaperone that can assist viral protein folding (21, 24), we also evaluated whether it could be playing an intracellular chaperoning role upon SARS-CoV-2 internalization. For this purpose, we added HM03 either before infection or after viral adsorption. The inhibition of GRP78 led to a decrease in viral copies, indicating that these receptors are indeed related to the entry of SARS-CoV-2 into hepatocytes (Fig. 4*C*). Also, the reduction observed with the postinfection inhibition of GRP78 suggested that this transporter could exert a role as a viral chaperone into hepatocytes upon SARS-CoV-2 infection. Of note, ACE2 blockade and pharmacological inhibition of GRP78 partially reduced the viral copy number and the number of infectious viral particles generated (Fig. 4*D*), while the combination of both ACE2 and GRP78 blockers does not yield an additive effect and diminished the effects of individual blockades (Fig. 4*D*). Furthermore, we also detected that ACE2 or GRP78 blockade normalized induction of glucose production upon viral infection to control levels; however, the simultaneous blockade of both receptors also

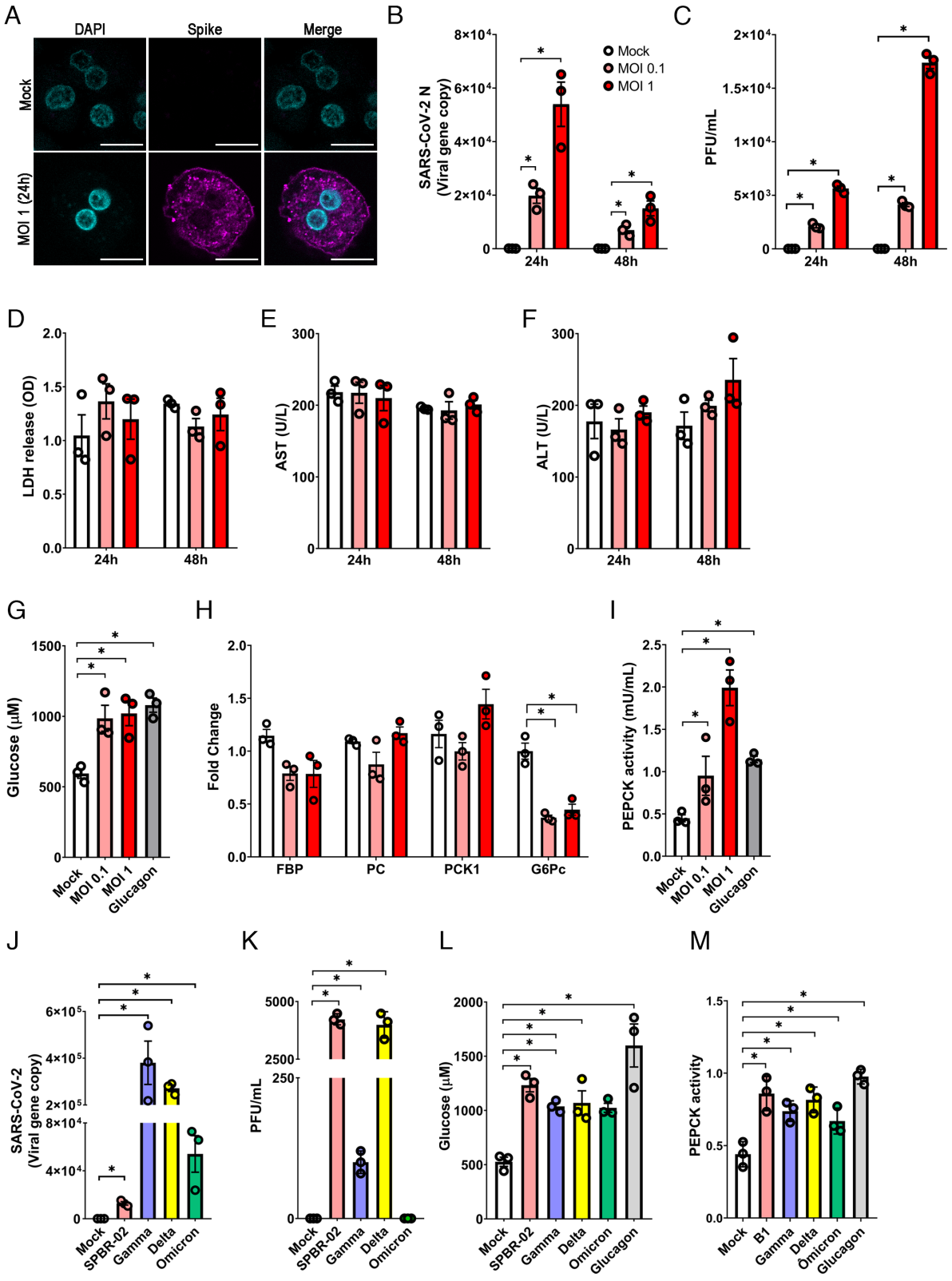

Fig. 2. Evaluation of SARS-CoV-2 in vitro infection in primary hepatocytes. (*A*) Representative immunofluorescence of human primary hepatocyte at MOI 1 for 24 h after infection. Blue—DAPI (nuclear marker). Magenta—SARS-COV-2 spike. (Scale bar: 60 μm.) Quantification of viral RNA (*B*) in human primary hepatocytes lysate and, quantification of plaque-forming units (*C*), LDH (lactate dehydrogenase) (*D*), AST (aspartate aminotransferase) (*E*), and ALT (alanine aminotransferase) (*F*) in the media of primary hepatocytes infected with SARS-CoV-2 variant SPBR-02 at MOIs of 0.1 and 1 after 24 h and 48 h. Glucose levels (*G*), expression of gluconeogenesis genes (*H*), and PEPCK activity (*I*) in primary hepatocytes infected with SARS-CoV-2 at MOIs of 0.1 and 1 at 48 h post infection. Viral RNA dosage at infection in different variants (SPBR-02, gamma, delta, omicron) of SARS-CoV-2 at MOI of 0.1 after 48 h (*J*). Plaque-forming units of supernatant of primary hepatocytes infected with SARS-CoV-2 with different variants of SARS-CoV-2 at MOIs of 0.1 and 1 after 48 h (*K*). Glucose levels (*L*) and PEPCK activity (*M*) in primary hepatocytes infected with different SARS-CoV-2 variants at MOI of 0.1 at 48 h post infection. ANOVA followed by Bonferroni post-hoc test was performed. Data are presented as mean ± SEM. *$P < 0.05$. In vitro data are representative of the N of three biological replicates, each performed in triplicate.

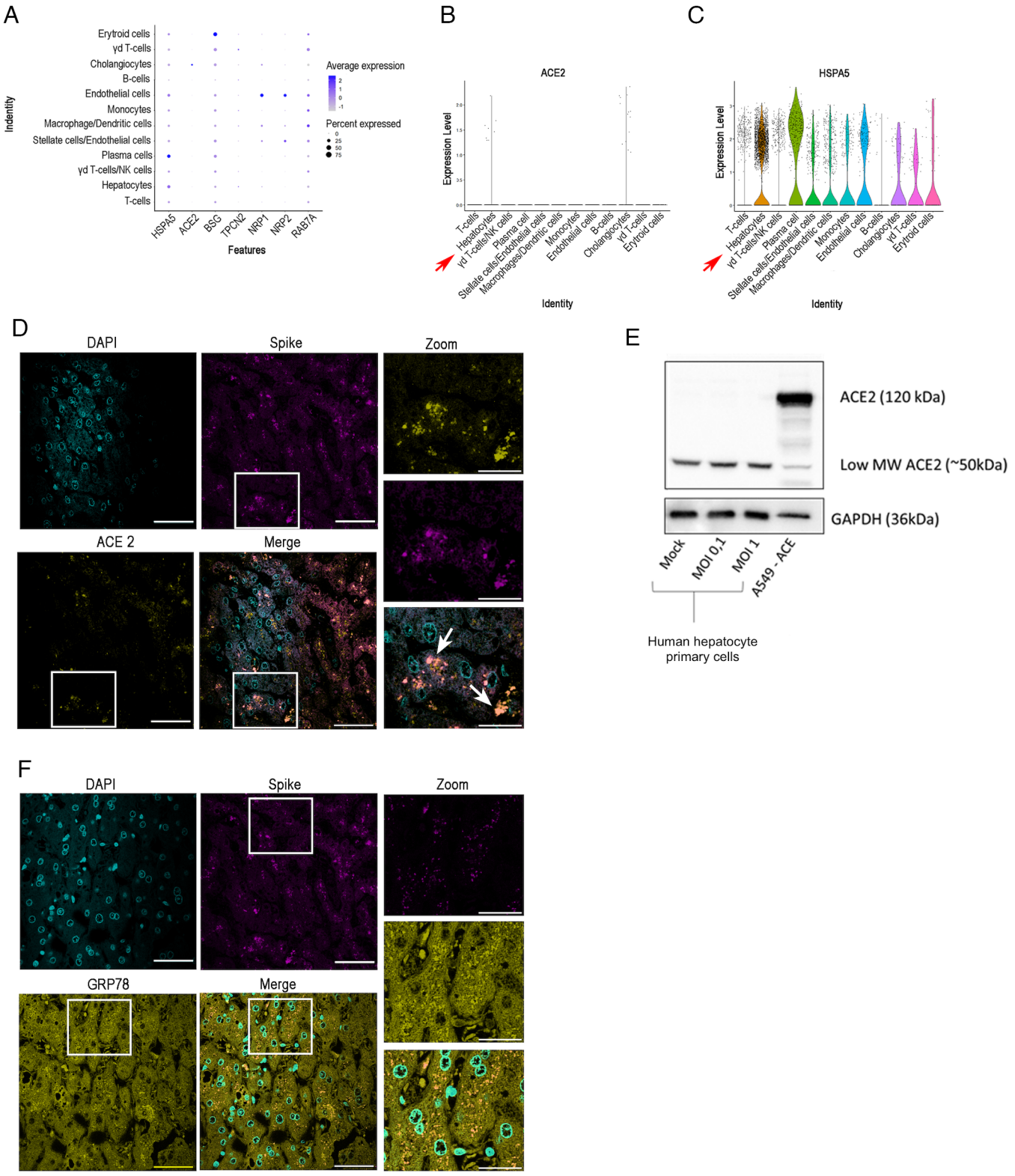

Fig. 3. Proteins related to SARS-CoV-2 entry into the different cell types of the liver. Human liver single-cell sequencing data were analyzed to identify the clusters of single populations and gene expression of proteins related to SARS-CoV-2 entry (*A*). The size of the circle represents the percentage of gene expression in the indicated cell types, while the color scale refers to the average expression. The expression distribution of ACE2 (*B*) and HSPA5 genes (*C*). Representative immunofluorescence of the human liver from autopsy of a COVID-19 patient (*D*). Arrows indicate sites of colocalization between spike and ACE2. Cyan – DAPI, yellow–ACE2, magenta–SARS-CoV-2 spike protein. (Scale bar: 50 μm.) Western blot of primary human hepatocytes infected with SARS-CoV-2 at MOIs of 0.1 and 1 and in ACE2 overexpressing A549 cells (*E*). Representative immunofluorescence of the human liver from a COVID-19 patient (*F*). Arrows indicate sites of colocalization between spike and GRP78. Cyan–DAPI, yellow—GRP78, magenta–SARS-COV-2 spike protein. (Scale bar: 50 μm.) *$P < 0.05$. In vitro data are representative of the N of three biological replicates, each performed in triplicate.

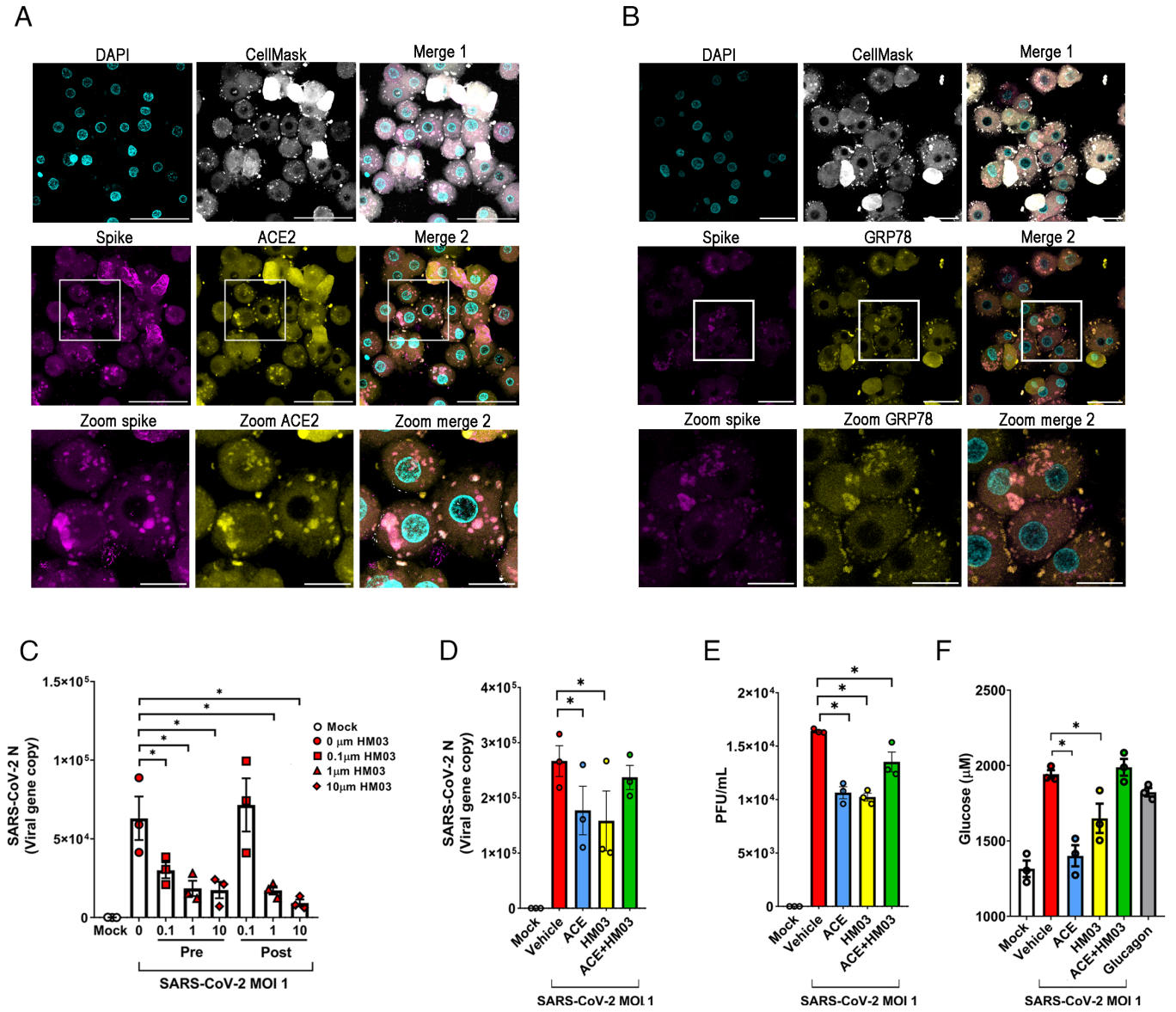

Fig. 4. ACE2 and GRP78 are involved in SARS-CoV-2 entry into hepatocytes. Immunofluorescence staining for ACE2 (*A*), or GRP78 (*B*), with spike protein and CellMask labeling in human hepatocytes infected with SARS-CoV-2 at MOI 0.1 for 50 min. Cyan–DAPI, magenta–viral spike protein, yellow–GRP78, white–CellMask. (Scale bar: 50 μm.) Viral dosage in primary hepatocytes infected with SARS-CoV-2 variant SPBR-02 in MOI of 1 treated with different concentrations of the GRP78 inhibitor (0.1, 1, and 10 μM) 1 h pre- or 24 h post-infection (*C*). Quantification of viral copies (*D*), plaque-forming unit assay (*E*), and glucose release (*F*) in primary human hepatocytes pretreated or not with the neutralizing anti-ACE2 antibody, or HM03, or with the combination of both. ANOVA followed by Bonferroni post-hoc test was performed. Data are presented as mean ± SEM. $*P < 0.05$. In vitro data are representative of the N of three biological replicates, each performed in triplicate.

prevented this inhibitory effect. These results suggests that ACE2 and GRP78 serve as viral transporters that likely cooperate for the viral internalization in hepatocytes and also indicate the presence of another compensatory mechanism in the absence of both transporters.

Discussion

We combined a retrospective clinical study with ex vivo and in vitro experimental approaches to show that COVID-19 is independently associated with the onset of hyperglycemia. We propose that this occurs as a result of the direct action of the virus in hepatocytes. Supporting a potential role of liver infection in COVID-19-induced hyperglycemia, we detected replicating infectious viruses in human hepatocytes. We also showed that infected hepatocytes increase glucose production, and this is associated with the stimulation of PEPCK activity. Furthermore, our results demonstrate that SARS-CoV-2 entry in hepatocytes partially occurs through ACE2- and GRP78-dependent mechanisms.

In-hospital COVID-19-related increase in blood glucose has been observed in previous studies and is related to worse outcomes (3). Most studies associated the highest daily glycemic values with higher length of hospital stay (4–5, 8), ICU admission rate (6), ventilation (25), and mortality rate (8, 24–26). Reiterer et al. (8) monitored glucometabolic profile of COVID-19-positive patients and reported that the incidence of insulin resistance and hyperglycemia was associated with the presence of acute respiratory distress syndrome. Our retrospective clinical study design differs from these previous studies as we aimed to understand whether COVID-19 is independently associated with in-hospital hyperglycemia when compared to a cohort of COVID-19-negative patients admitted at the same period for other pathologies and who were also kept at ICU at the same proportion as the COVID-19-positive group.

Whether COVID-19-induced dysglycemia could be due to SARS-CoV-2 infection in the pancreas is still controversial. In vitro viral infection of beta cells causing cell death and defective insulin secretion has been shown (5, 7, 27–30). Herein, we observed that hyperglycemic COVID-19 patients display increased c-peptide and glycated serum protein levels compared to COVID-19 normoglycemic and negative patients at hospital admission. We have chosen to use samples collected at the admission day because that was the only time in which we were sure that none of the patients were under glucocorticoid therapy. The concomitant increase in blood glucose, glycated proteins, and c-peptide in COVID-19 patients may suggest that these individuals were already displaying some degree of insulin resistance at admission as a consequence of the infection but did not display a compromised pancreatic function. Even though the elevated glycated serum protein levels in COVID+ HG group can reflect the alterations within the past 2 to 3 wk, this parameter is also likely affected by the rise in blood glucose undergone by the patients after viral infection. Important to mention that the lack of a HbA1c assessment is a limitation of this study, since it could better predict patient's glycemic status during the 2 to 3 mo preceding the viral infection. Other studies also showed that COVID-19 patients have elevated levels of c-peptide compared with non-COVID-19 patients (5, 8, 31–33).

Previously published studies have already shown liver infection by SARS-CoV-2 as a cause of hepatic damage under COVID-19 (12, 34–39). Interestingly, one of these studies demonstrated that SARS-CoV-2-infected liver partially shared the gene expression profile of HCV, HBV, and HIV infections. This study also detected spike protein in hepatocytes (12); however, it did not demonstrate whether the infection was productive. Our study shows that SARS-CoV-2 can infect, replicate, and produce infectious viral particles in primary human hepatocytes, while providing evidences that it is possibly occurring in the liver from COVID-19 patients as well. Also, we did not find cellular damage after in vitro infection, which contrasts with other studies that found increased histopathological (34–38) and serological (39) liver damage markers. The fact that we evaluated acute infection in cells without a liver microenvironment may justify this discrepancy.

The COVID-19 waves showed differences in clinical pattern and severity (40, 41) as they were caused by SARS-CoV-2 variants that differ in pathogenicity (42). Given these substantial differences, we decided to assess whether the other variants could phenocopy the original strain effects in hepatocytes. Interestingly, the production rate of infectious viral particles is higher in SPBR-02 and delta than that in gamma, while it was undetected in omicron infection. These findings highlight the lower pathogenicity of omicron, regardless of its capacity to infect cells, as previously reported (43, 44). Indeed, omicron's lower capacity to form plaques in vitro was previously reported and attributed to its lower fusogenicity (45). Interestingly, omicron infection induced gluconeogenesis in hepatocytes while the inactive virus did not. It may suggest that omicron can still replicate into the cells and trigger a gluconeogenic signaling pathway, although it is not capable of producing viable viral particles. The participation of replication intermediates in the mechanism of gluconeogenesis in hepatocytes warrants further investigation.

To understand the potential causes of hyperglycemia in COVID-19, we wondered whether SARS-CoV-2 infection in hepatocytes leads to gluconeogenesis. Our data showed that infected hepatocytes produce more glucose than that of the uninfected controls. Previous study has shown that COVID-19 induced the increase of the glucogenic hormone GP73 that was capable of promoting glucose production in Huh7 cells while increasing gene expression of gluconeogenic genes (13). In contrast, we found that the infection of primary human hepatocytes with SARS-CoV-2 increased PEPCK activity but not gene expression. This discrepancy may be explained by the fact that we used primary hepatocytes while they used hepatoma cells, which are largely modified at both phenotypic and genotypic levels. The unchanged expression of gluconeogenesis or glycogenolysis pathways agrees with previously published liver proteomics studies in COVID-19 patients (12, 46, 47). PEPCK activity can also be modulated by posttranslational regulation through acetylation of residues Lys-19 and Lys-514 (48), which might be a potential mechanism underlying its induction upon SARS-CoV-2 infection. The elucidation of the signaling pathways regulating PEPCK activity in response to SARS-CoV-2 infection warrants further investigation.

SARS-CoV-2 infection in hepatocytes is still a controversial topic, since preliminary evidence from scRNAseq analysis indicated that *ACE2* is expressed at very low levels in hepatocytes (17). In fact, our scRNAseq analysis from a public dataset corroborated these findings from the literature. However, we found that hepatocytes express the short ACE2 isoform, which was previously reported to lack many residues previously shown to be important for viral binding, thereby resulting in a low shuttling capacity. This may explain our data that the ACE2 blockade only partially reduces virus entry into the cell. In addition, the scRNAseq analysis also revealed GRP78 as the SARS-CoV-2 entry factor expressed at the highest levels in hepatocytes. GRP78 is an endoplasmic reticulum chaperone that can also be translocated to the cell surface, especially under stress conditions (49). GRP78 was previously reported as an auxiliary receptor for SARS-CoV-2 entry (20, 50). Our findings show that both ACE2 and GRP78 colocalizes with spike protein at cell membrane, and their individual blockades significantly impede virus entrance in hepatocytes. However, the concomitant blockade of both receptors did not result in additive or synergistic blocking effect, reinforcing the evidence that these receptors likely cooperate in the same pathway for internalizing the virus. Curiously, when the receptors were simultaneously blocked, there was a mitigation of the blocking effect, suggesting that there is an alternative pathway that operates in parallel and compensates for the absence of GRP78 and ACE2 action. In fact, several other receptors were described for SARS-CoV-2 in different tissues and/or cell lines, which may need to be further investigated in hepatocytes.

In conclusion, our data evidence that SARS-CoV-2 is a direct trigger of hepatic glucose production, which in turn may contribute to the hyperglycemia observed in COVID-19 patients. We showed that all the variants of concern are able to infect hepatocytes and increase hepatic gluconeogenesis associated with PEPCK activity. This study also demonstrates that the cooperation of the transporters GRP78 and the short ACE2 isoform is partially responsible for SARS-CoV-2 entry into hepatocytes, while an unidentified shuttling mechanism may also mediate viral internalization in a parallel pathway. Our results shed light into an important aspect underlying COVID-19 pathophysiology that is the need for a better control of hepatic glucose production in order to achieve a better glycemic control, thus protecting COVID-19 patients against the deleterious impact of in-hospital hyperglycemia for their clinical outcomes.

Data, Materials, and Software Availability. All study data are included in the article and/or *SI Appendix*.

ACKNOWLEDGMENTS. We thank our lab technicians, administrative staff, and specially the virology section for kindly providing all the support needed for handling viruses under safe conditions. This study was supported by grants from São

Paulo Research Foundation (FAPESP, grant nos. 2020/05040-4, 2017/08264-8, 2016/00194-8, and 2020/04558-0).

Author affiliations: [a]Department of Pharmacology, Ribeirão Preto Medical School, University of São Paulo, Ribeirão Preto 14049-900, Brazil; [b]Center for Research in Inflammatory Diseases, Ribeirão Preto Medical School, University of São Paulo, Ribeirão Preto 14049-900, Brazil; [c]Department of Cell Biology, Ribeirão Preto Medical School, University of São Paulo, Ribeirão Preto 14049-900, Brazil; [d]Federal University of Paraná, Center for Study and Research in Intensive Care Medicine, Curitiba 82530-200, Brazil; [e]Department of Pathology and Legal Medicine, Ribeirão Preto Medical School, University of São Paulo, Ribeirão Preto 14049-900, Brazil; [f]Hospital Israelita Albert Einstein, São Paulo 05652-900, Brazil; [g]Department of Biochemistry and Tissue Biology, Institute of Biology, University of Campinas, Campinas 13083-970, Brazil; [h]Department of Genetics, Microbiology and Immunology, Laboratory of Emerging Viruses, Institute of Biology, University of Campinas, Campinas 13083-970, Brazil; [i]Experimental Medicine Research, Cluster University of Campinas, Campinas 13083-970, Brazil; [j]Obesity and Comorbidities Research Center, University of Campinas, Campinas 13083-864, Brazil; [k]Divisions of Clinical Immunology, Emergency, Infectious Diseases, and Intensive Care Unit, Ribeirão Preto Medical School, University of São Paulo, Ribeirão Preto 14049-900, Brazil; and [l]Hospital de Clínicas da Universidade Federal do Paraná, Curitiba 80060-900, Brazil

Author contributions: M.M.F.d.S. and L.O.L. designed research; E.A.B., A.S.C., F.P.V., R.M., R.S.B., I.M.P., T.M.L., R.C.G., S.D., N.P., J.M.A., T.T.G., J.F., S.P.M., G.F.D., S.S.B., M.M.F.d.S., and L.O.L. performed research; R.M., J.L.P.-M., M.A.M., F.Q.C., P.L.-J., T.M.C., A.F., R.D.R.d.O., E.A., R.R., Á.R.N., and L.O.L. contributed new reagents/analytic tools; E.A.B., F.P.V., R.S.B., I.M.P., T.M.L., Y.S., T.T.G., J.L.P.-M., P.L.-J., H.I.N., R.D.R.d.O., R.R., Á.R.N., M.M.F.d.S., and L.O.L. analyzed data; and E.A.B., J.M.P., M.A.M., F.Q.C., T.M.C., A.F., E.A., M.M.d.S.F., and L.O.L. wrote the paper.

1. F. Zho *et al.*, Clinical course and risk factors for mortality of adult inpatients with COVID-19 in Wuhan, China: A retrospective cohort study. *Lancet* **395**, 1054–1062 (2020).
2. N. Stefan, A. L. Birkenfeld, M. B. Schulze, Global pandemics interconnected–Obesity, impaired metabolic health and COVID-19. *Nat. Rev. Endocrinol.* **17**, 135–149 (2021).
3. Y. Yang, Z. Cai, J. Zhang, Hyperglycemia at admission is a strong predictor of mortality and severe/critical complications in COVID-19 patients: A meta-analysis. *Biosci. Rep.* **41**, BSR20203584 (2021).
4. S. Mirabella *et al.*, Glucose dysregulation and its association with COVID-19 mortality and hospital length of stay. *Diabetes Metab. Syndr. Clin. Res. Rev.* **16**, 102439 (2022).
5. L. Montefusco *et al.*, Acute and long-term disruption of glycometabolic control after SARS-CoV-2 infection. *Nat. Metab.* **3**, 774–785 (2021).
6. C. Steenblock *et al.*, Viral infiltration of pancreatic islets in patients with COVID-19. *Nat. Commun.* **12**, 3534 (2021).
7. C.-T. Wu *et al.*, SARS-CoV-2 infects human pancreatic β cells and elicits β cell impairment. *Cell Metab.* **33**, 1565–1576.e5 (2021).
8. M. Reiterer *et al.*, Hyperglycemia in acute COVID-19 is characterized by insulin resistance and adipose tissue infectivity by SARS-CoV-2. *Cell Metab.* **33**, 2174–2188.e5 (2021).
9. J. Chen *et al.*, The metabolic regulator histone deacetylase 9 contributes to glucose homeostasis abnormality induced by hepatitis C virus infection. *Diabetes* **64**, 4088–4098 (2015).
10. H.-J. Jhuang *et al.*, Gluconeogenesis, lipogenesis, and HBV replication are commonly regulated by PGC-1α-dependent pathway. *Oncotarget* **6**, 7788–7803 (2015).
11. Y. Wang *et al.*, SARS-CoV-2 infection of the liver directly contributes to hepatic impairment in patients with COVID-19. *J. Hepatol.* **73**, 807–816 (2020).
12. N. Wanner, Molecular consequences of SARS-CoV-2 liver tropism. *Nat. Metab.* **4**, 310–319 (2022). Accessed 25 May 2022.
13. L. Wan, GP73 is a glucogenic hormone contributing to SARS-CoV-2-induced hyperglycemia. *Nat. Metab.* **4**, 29–43 (2022). Accessed 26 May 2022.
14. M. C. Pontelli *et al.*, SARS-CoV-2 productively infects primary human immune system cells in vitro and in COVID-19 patients. *J. Mol. Cell Biol.* **14**, mjac021 (2022).
15. S. A. MacParland *et al.*, Single cell RNA sequencing of human liver reveals distinct intrahepatic macrophage populations. *Nat. Commun.* **9**, 4383 (2018).
16. J. S. Krinsley, Association between hyperglycemia and increased hospital mortality in a heterogeneous population of critically Ill patients. *Mayo Clin. Proc.* **78**, 1471–1478 (2003).
17. F. Qi, Single cell RNA sequencing of 13 human tissues identify cell types and receptors of human coronaviruses. *Biochem. Biophys. Res. Commun.* **526**, 135–140 (2020). Accessed 25 May 2022.
18. K. F. R. Pobre, G. J. Poet, L. M. Hendershot, The endoplasmic reticulum (ER) chaperone BiP is a master regulator of ER functions: Getting by with a little help from ERdj friends. *J. Biol. Chem.* **294**, 2098–2108 (2019). Accessed 26 May 2022.
19. I. M. Ibrahim, D. H. Abdelmalek, A. A. Elfiky, GRP78: A cell's response to stress. *Life Sci.* **226**, 156–163 (2019).
20. A. J. Carlos, The chaperone GRP78 is a host auxiliary factor for SARS-CoV- 2 and GRP78 depleting antibody blocks viral entry and infection. *J. Biol. Chem.* **296** 100759–100760 (2021). Accessed 25 May 2022.
21. D. P. Ha, The stress-inducible molecular chaperone GRP78 as potential therapeutic target for coronavirus infection. *J. Infect.* **81**, 452 (2020). Accessed 26 May 2022.
22. F. P. Veras *et al.*, SARS-CoV-2-triggered neutrophil extracellular traps mediate COVID-19 pathology. *J. Exp. Med.* **217**, e20201129 (2020).
23. M. Huang *et al.*, Structure-based design of HSPA5 inhibitors: From peptide to small molecule inhibitors. *Bioorg. Med. Chem Lett.* **23**, 3044–3050 (2013).
24. J. O. Rayner *et al.*, AR12 (OSU-03012) suppresses GRP78 expression and inhibits SARS-CoV-2 replication. *Biochem. Pharmacol.* **182**, 114227 (2020).
25. J. M. Bhatti, Association between glycemic control and the outcome in hospitalized patients with COVID-19. *Endocrine* **77**, 213–220 (2022). Accessed 26 May 2022.
26. J. Wu *et al.*, Elevation of blood glucose level predicts worse outcomes in hospitalized patients with COVID-19: A retrospective cohort study. *BMJ Open Diabetes Res. Care* **8**, e001476 (2020).
27. K. C. Coate *et al.*, SARS-CoV-2 cell entry factors ACE2 and TMPRSS2 are expressed in the microvasculature and ducts of human pancreas but are not enriched in β cells. *Cell Metab.* **32**, 1028–1040.e4 (2020).
28. J. A. Müller *et al.*, SARS-CoV-2 infects and replicates in cells of the human endocrine and exocrine pancreas. *Nat. Metab.* **3**, 149–165 (2021).
29. M. M. F. Qadir *et al.*, SARS-CoV-2 infection of the pancreas promotes thrombofibrosis and is associated with new-onset diabetes. *JCI Insight* **6**, e151551 (2021).
30. X. Tang *et al.*, SARS-CoV-2 infection induces beta cell transdifferentiation. *Cell Metab.* **33**, 1577–1591.e7 (2021).
31. R. Robeva *et al.*, C-peptide levels and glycemic indices in COVID-19 patients. *Biotechnol. Biotechnol. Equip.* **36**, 418–424 (2022), 10.1080/13102818.2022.2090858.
32. I. Ilias *et al.*, Glycemia, beta-cell function and sensitivity to insulin in mildly to critically Ill Covid-19 patients. *Medicina (kaunas)* **57**, 68 (2021).
33. L. Bergantini *et al.*, Prognostic bioindicators in severe COVID-19 patients. *Cytokine* **141**, 155455 (2021).
34. B. Hanley *et al.*, Histopathological findings and viral tropism in UK patients with severe fatal COVID-19: A post-mortem study. *Lancet Microbe.* **1**, e245–e253 (2020).
35. V. G. Puelles *et al.*, Multiorgan and renal tropism of SARS-CoV-2. *N. Engl. J. Med.* **383**, 590–592 (2020).
36. B. T. Bradley *et al.*, Histopathology and ultrastructural findings of fatal COVID-19 infections in Washington State: A case series. *Lancet* **396**, 320–332 (2020).
37. S. M. Lagana *et al.*, Hepatic pathology in patients dying of COVID-19: A series of 40 cases including clinical, histologic, and virologic data. *Mod. Pathol.* **33**, 2147–2155 (2020).
38. S. S. Elsoukkary *et al.*, Autopsy findings in 32 patients with COVID-19: A single-institution experience. *Pathobiology* **88**, 56–68 (2020).
39. M. P. Kumar *et al.*, Coronavirus disease (COVID-19) and the liver: A comprehensive systematic review and meta-analysis. *Hepatol. Int.* **14**, 711–722 (2020), 10.1007/s12072-020-10071-9.
40. C. Maslo *et al.*, Characteristics and outcomes of hospitalized patients in south africa during the COVID-19 omicron wave compared with previous waves. *JAMA* **327**, 583 (2022).
41. K. A. Twohig *et al.*, Hospital admission and emergency care attendance risk for SARS-CoV-2 delta (B.1.617.2) compared with alpha (B.1.1.7) variants of concern: A cohort study. *Lancet Infect. Dis.* **22**, 35–42 (2022).
42. B. Stolp *et al.*, SARS-CoV-2 variants of concern display enhanced intrinsic pathogenic properties and expanded organ tropism in mouse models. *Cell Rep.* **38**, 110387 (2022).
43. H. Shuai *et al.*, Attenuated replication and pathogenicity of SARS-CoV-2 B.1.1.529 Omicron. *Nature* **603**, 693–699 (2022).
44. K. P. Y. Hui *et al.*, SARS-CoV-2 Omicron variant replication in human bronchus and lung ex vivo. *Nature* **603**, 715–720 (2022).
45. R. Suzuki *et al.*, Attenuated fusogenicity and pathogenicity of SARS-CoV-2 Omicron variant. *Nature* **603**, 700–705 (2022).
46. L. Leng *et al.*, Pathological features of COVID-19-associated liver injury–a preliminary proteomics report based on clinical samples. *Signal Transduct. Target. Ther.* **6**, 9 (2021).
47. X. Nie *et al.*, Multi-organ proteomic landscape of COVID-19 autopsies. *Cell* **184**, 775–791.e14 (2021).
48. Y. Lin *et al.*, Protein acetylation microarray reveals that NuA4 controls key metabolic target regulating gluconeogenesis. *Cell* **136**, 1073–1084 (2009). Accessed 31 May 2022.
49. M. Gonzalez-Gronow *et al.*, GRP78: A multifunctional receptor on the cell surface. *Antioxid. Redox. Signal* **11**, 2299–2306 (2009), 10.1089/ars.2009.2568.
50. L. Allam *et al.*, Targeting the GRP78-dependant SARS-CoV-2 Cell entry by peptides and small molecules. *Bioinform. Biol. Insights* **14**, 117793222096550 (2020), 10.1177/1177932220965505.